

Original Article



OPEN ACCESS

Received: Feb 2, 2025

Revised: Mar 11, 2025

Accepted: Mar 25, 2025

Published online: Apr 9, 2025

Correspondence to

Jaeho Kim

Department of Neurology, Dongtan Sacred Heart Hospital, Hallym University College of Medicine, 7 Keunjaebong-gil, Hwaseong 18450, Korea.

Email: jaehokim@hallym.ac.kr

Kichang Kwak

BeauBrain Healthcare, Inc., 314 Hakdong-ro, Gangnam-gu, Seoul 06098, Korea.

Email: kichang.kwak@beaubrain.bio

*These authors contributed equally to this article as co-first authors.

© 2025 Korean Dementia Association

This is an Open Access article distributed under the terms of the Creative Commons Attribution Non-Commercial License (<https://creativecommons.org/licenses/by-nc/4.0/>) which permits unrestricted non-commercial use, distribution, and reproduction in any medium, provided the original work is properly cited.

ORCID iDs

Seongbeom Park

<https://orcid.org/0000-0002-0759-6826>

Kyoungmin Kim

<https://orcid.org/0009-0000-4161-3573>

Soyeon Yoon

<https://orcid.org/0009-0003-9439-1152>

Seongmi Kim

<https://orcid.org/0009-0004-3144-9908>

Jehyun Ahn

<https://orcid.org/0009-0008-0927-6069>

Establishing Regional A β Cutoffs and Exploring Subgroup Prevalence Across Cognitive Stages Using BeauBrain Amylo[®]

Seongbeom Park ^{1,*}, Kyoungmin Kim ^{2,*}, Soyeon Yoon ², Seongmi Kim ²,
Jehyun Ahn ², Kyoung Yoon Lim ¹, Hyemin Jang ³, Duk L. Na ^{1,4},
Hee Jin Kim ^{2,5,6,7,8}, Seung Hwan Moon ⁹, Jun Pyo Kim ⁵, Sang Won Seo ^{2,5,6,7,8},
Jaeho Kim ¹⁰, Kichang Kwak ¹

¹BeauBrain Healthcare, Inc., Seoul, Korea

²Alzheimer's Disease Convergence Research Center, Samsung Medical Center, Seoul, Korea

³Department of Neurology, Seoul National University Hospital, Seoul National University College of Medicine, Seoul, Korea

⁴Department of Neurology, Happymind Clinic, Seoul, Korea

⁵Department of Neurology, Samsung Medical Center, Sungkyunkwan University School of Medicine, Seoul, Korea

⁶Department of Health Sciences and Technology, SAIHST, Sungkyunkwan University, Seoul, Korea

⁷Department of Intelligent Precision Healthcare Convergence, Sungkyunkwan University, Suwon, Korea

⁸Department of Digital Health, SAIHST, Sungkyunkwan University, Seoul, Korea

⁹Department of Nuclear Medicine, Samsung Medical Center, Sungkyunkwan University School of Medicine, Seoul, Korea

¹⁰Department of Neurology, Dongtan Sacred Heart Hospital, Hallym University College of Medicine, Hwaseong, Korea

ABSTRACT










Background and Purpose: Amyloid-beta (A β) plaques are key in Alzheimer's disease (AD), with A β positron emission tomography imaging enabling non-invasive quantification. To address regional A β deposition, we developed regional Centiloid scales (rdcCL) and commercialized them through the computed tomography (CT)-based BeauBrain Amylo platform, eliminating the need for three-dimensional T1 magnetic resonance imaging (MRI).

Objective: We aimed to establish robust regional A β cutoffs using the commercialized BeauBrain Amylo platform and to explore the prevalence of subgroups defined by global, regional, and striatal A β cutoffs across cognitive stages.

Methods: We included 2,428 individuals recruited from the Korea-Registries to Overcome Dementia and Accelerate Dementia Research project. We calculated regional A β cutoffs using Gaussian Mixture Modeling. Participants were classified into subgroups based on global, regional, and striatal A β positivity across cognitive stages (cognitively unimpaired [CU], mild cognitive impairment, and dementia of the Alzheimer's type).

Results: MRI-based and CT-based global A β cutoffs were highly comparable and consistent with previously reported Centiloid values. Regional cutoffs revealed both similarities and differences between MRI- and CT-based methods, reflecting modality-specific segmentation processes. Subgroups such as global(-)regional(+) were more frequent in non-dementia stages, while global(+)striatal(-) was primarily observed in CU individuals.

Conclusions: Our study established robust regional A β cutoffs using a CT-based rdcCL method and demonstrated its clinical utility in classifying amyloid subgroups across

Kyoung Yoon Lim 
<https://orcid.org/0009-0006-5239-6424>
 Hyemin Jang 
<https://orcid.org/0000-0003-3152-1274>
 Duk L. Na 
<https://orcid.org/0000-0002-0098-7592>
 Hee Jin Kim 
<https://orcid.org/0000-0002-3186-9441>
 Seung Hwan Moon 
<https://orcid.org/0000-0003-4302-1920>
 Jun Pyo Kim 
<https://orcid.org/0000-0003-4376-3107>
 Sang Won Seo 
<https://orcid.org/0000-0002-8747-0122>
 Jaeho Kim 
<https://orcid.org/0000-0003-3770-2359>
 Kichang Kwak 
<https://orcid.org/0000-0003-4542-0001>

Funding

This research was supported by a grant from the Korea Health Technology R&D Project through the Korea Health Industry Development Institute (KHIDI), funded by the Ministry of Health & Welfare and Ministry of Science and ICT, Republic of Korea (grant number: HU20C0111); by a National Research Foundation of Korea (NRF) grant funded by the Korean government (MSIT) (NRF-2019R1A5A2027340); and by funds (2021-ER1006-00) from the Research of Korea Disease Control and Prevention Agency.

Conflict of Interest

The authors have no financial conflicts of interest.

Author Contributions

Conceptualization: Park S, Kim K, Jang H, Na DL, Kim HJ, Moon SH, Kim JP, Seo SW, Kim J, Kwak K; Data curation: Jang H, Na DL, Kim HJ, Moon SH, Kim JP; Investigation: Yoon S, Kim S, Ahn J; Methodology: Lim KY; Supervision: Seo SW, Kwak K; Writing - original draft: Park S; Writing - review & editing: Seo SW, Kim J, Kwak K.

cognitive stages. These findings highlight the importance of regional A β quantification in understanding amyloid pathology and its implications for biomarker-guided diagnosis and treatment in AD.

Keywords: Alzheimer Disease; Tomography, X-Ray Computed; Positron-Emission Tomography; Cognition Disorders; Amyloid Plaques

INTRODUCTION

Alzheimer's disease (AD) is characterized by the accumulation of amyloid-beta (A β) plaques in the brain, which begins years before the onset of clinical symptoms.¹⁻⁴ The advent of A β positron emission tomography (PET) imaging has provided a non-invasive in vivo method to detect amyloid deposition, offering valuable insights into the pathophysiological stages of AD.⁵⁻⁹ Studies have shown that the prevalence of amyloid positivity increases across cognitive stages, from approximately 20%–40% in cognitively unimpaired (CU) individuals to 50%–60% in those with mild cognitive impairment (MCI) and over 80% in dementia of the Alzheimer's type (DAT).^{10,11} While visual assessments remain widely used for A β PET interpretation, quantification pipelines offer more objective and reproducible results, emphasizing the need for comparative studies to evaluate these methods.

To standardize amyloid quantification across different PET ligands, the Centiloid (CL) method was introduced, enabling the harmonization of 11C-labeled Pittsburgh compound B and 18F-labeled A β PET tracers through a common scale.^{7,12,15} This approach has greatly enhanced cross-study comparability and clinical utility in AD research. However, traditional CL methods primarily focus on a global measure of A β burden, potentially overlooking regional variations that can provide critical insights into disease progression.

Recent evidence underscores the need to examine such regional variations in A β deposition. For instance, some individuals with globally amyloid-negative scans may still exhibit regional amyloid positivity, which has been associated with subtle cognitive changes¹⁶ and an increased likelihood of conversion to global amyloid positivity.¹⁷ Conversely, for globally amyloid-positive individuals, striatal involvement has been linked to worse clinical outcomes, highlighting the importance of assessing both global and region-specific amyloid patterns.^{16,18,19} Furthermore, CL values are increasingly used in the context of Food and Drug Administration-approved amyloid-targeting therapies, aiding in patient selection, treatment monitoring, and identifying those most likely to benefit from these treatments.²⁰⁻²³

To address the limitations of a purely global approach, our group developed regional Centiloid scales (rdcCL) that harmonize A β uptake across various PET ligands using computed tomography (CT) images acquired during PET-CT scans for anatomical reference.²⁴ By eliminating the need for additional three-dimensional (3D) T1 magnetic resonance imaging (MRI) data, this method simplifies the analytic process and broadens its applicability in both clinical and research settings. Previous studies have validated the pathological and clinical utility of rdcCL, showing that it effectively detects region-specific A β deposition and can distinguish clinical phenotypes relevant to AD progression.^{16,19}

Building on these findings, we developed BeauBrain Amylo, a platform designed to standardize and implement rdcCL for broader clinical and research use. A key advantage of

BeauBrain Amylo is its ability to derive regional A β measures from CT-based registration alone, thereby removing the need for separate 3D T1 MRI acquisitions. In this study, we aim to establish robust regional A β cutoffs using this platform and to explore the prevalence of subgroups defined by global, regional, and striatal A β cutoffs across cognitive stages (CU, MCI, and DAT). Through this work, we hope to deepen our understanding of amyloid pathology and its clinical implications, ultimately paving the way for more precise diagnostics and targeted interventions in AD.

METHODS

Participants selection

This study included 2,428 individuals recruited from the Korea-Registries to Overcome Dementia and Accelerate Dementia Research (K-ROAD) project,²⁵ which is a member of the Worldwide Alzheimer's Disease Neuroimaging Initiative. The K-ROAD project aimed to establish a genotype–phenotype cohort to accelerate the development of innovative diagnostic and therapeutic techniques for neurodegenerative diseases, mainly AD and related dementia syndromes, in collaboration with 25 nationwide university-affiliated hospitals in South Korea between 2016 and 2023. All participants displayed one or more of the following: CU, MCI, and DAT. CU participants (n=581) were selected based on following criteria: (1) absence of medical history that is likely to affect cognitive function based on Christensen's health screening criteria²⁶ and (2) absence of objective cognitive impairment observed on any cognitive domain (above the -1.0 standard deviation [SD] of age- and education-matched norms in memory and above -1.5 SD in other cognitive domains).²⁷ Participants with MCI (n=931) met the specified criteria²⁸: (1) subjective cognitive complaints by the participants or caregiver; (2) objective cognitive impairment in any cognitive domain (below the -1.0 SD of age- and education-matched norms in memory and/or below -1.5 SD in other cognitive domains); (3) no significant impairment in activities of daily living; and (4) no dementia. Participants diagnosed with DAT (n=645) fulfilled the National Institute on Aging and Alzheimer's Association diagnostic criteria.²⁹ The "others" group included a total of 271 participants, comprising 258 with vascular cognitive impairment (VCI), 9 with frontotemporal dementia (FTD), and 4 with dementia with Lewy bodies (DLB). These diagnoses were based on established criteria, including the National Institute of Neurological Disorders and Stroke and the Association Internationale pour la Recherche et l'Enseignement en Neurosciences criteria for VCI,³⁰ the International Consensus Criteria for FTD,³¹ and the Fourth Consensus Report of the DLB Consortium for DLB.³² This approach ensured consistency with standard diagnostic guidelines in neurodegenerative and vascular conditions.

All participants underwent clinical interviews, neurological examinations, neuropsychological testing, and brain MRI. After these evaluations, clinical diagnoses were determined through agreement among a multidisciplinary team. Furthermore, all participants underwent blood tests, including complete blood counts, blood chemistry tests, vitamin B12/folate measurement, thyroid function test, and syphilis serology, to rule out the possibility of medical conditions causing cognitive decline, and APOE genotyping. Patients were excluded if they had territorial infarctions, brain tumors, or vascular malformations on MRI. Patients with white matter hyperintensities caused by radiation injury, vasculitis, multiple sclerosis, or leukodystrophy were also excluded.

The Institutional Review Board (IRB) of Samsung Medical Center approved the study protocol (IRB approval No. 2021-02-135), and all methods were performed according to the approved guidelines. Written consent was obtained from each participant.

MRI data acquisition

Standardized 3D T1 turbo field echo images were acquired from all participants at Samsung Medical Center using the same 3.0 T MRI scanner (Philips Achieva; Philips Healthcare, Andover, MA, USA). The detailed parameters were as follows: sagittal slice thickness, 1.0 mm, over contiguous slices with 50% overlap; no gap; repetition time of 9.9 ms; echo time of 4.6 ms; flip angle of 8°, and matrix size of 240×240 pixels, reconstructed to 480×480 over a field of view of 240 mm.

A β PET-CT data acquisition

Participants underwent ¹⁸F-flutemetamol (FMM) and ¹⁸F-florbetaben (FBB) PET at Samsung Medical Center using a Discovery STe PET/CT scanner (GE Medical Systems, Milwaukee, WI, USA) in 3D scanning mode that examined 47 slices 3.3-mm in thickness spanning the entire brain.^{33,34} According to the protocols for the ligands proposed by the manufacturers, a 20-minute emission PET scan with dynamic mode (consisting of 4×5 minutes frames) was performed 90 minutes after injection of a mean dose of 185 MBq of FMM or 311.5 MBq of FBB. 3D PET images were reconstructed in a 128×128×47 matrix with a voxel size of 2 mm×2 mm×3.27 mm using the ordered-subsets expectation maximization algorithm (FMM iterations=4 and subset=20; FBB iterations=4 and subset=20).

CT images were acquired using a 16-slice helical CT (140 KeV, 80 mA; 3.75-mm section width) for attenuation correction and were reconstructed in a 512×512 matrix with a voxel size of 0.5 mm×0.5 mm×3.27 mm. The kernel (i.e., smoothing filter) size of 5 mm was used for FMM according to the vendor's recommendation. However, since there was no recommendation of smoothing for FBB, we did not do perform it.

Quantitative analysis of A β PET images

We employed BeauBrain Amylo (BeauBrain Healthcare, Inc., Seoul, Korea; beaubrain.bio) to automatically quantify A β binding in amyloid PET. This software provides fully automated calculations of standardized uptake value ratio (SUVR) and CL values, ensuring robust quantitative analysis applicable to both PET-CT and PET-MR images. The processing pipeline includes co-registration, spatial normalization to a template, atlas-based segmentation, and calculation of dcSUVR and rdcSUVR. Subsequently, dcCL and rdcCL scales are calculated for the global region as well as six specific regions: frontal, temporal, parietal, posterior cingulate (PC), occipital and striatum.¹⁹ For CT images, and additional Hounsfield unit correction step is included as part of the preprocessing.

Defining subgroups by global, regional, and striatal A β cutoffs

The group was classified into four groups based on global and striatal rdcCL cutoffs. Initially, the participants were classified into 2 subgroup based on global A β rdcCL scales, which reflect the amyloid burden in the global region: global (−) and global (+). The global (−) group was further subdivided into regional (−) and regional (+) groups according to regional cutoffs for at least one region. Similarly, the global (+) group was divided into striatal (−) and striatal (+) groups based on striatal cutoffs. Thus, the cohort was classified into 4 groups: global (−) and regional (−) A β : G(−)R(−), global (−) and regional (+) A β : G(−)R(+), global (+) and striatal (−) A β : G(+)Str(−), and global (+) and striatal (+) A β : G(+)Str(+).

Table 1. Participant demographics and clinical findings

Variables	Total	CU	MCI	DAT	Others
No. of participants	2,428	581	931	645	271
Age (yr)	71.2 \pm 9.5	69 \pm 10.6	72 \pm 8.2	70 \pm 10.2	76 \pm 7.1
Sex (F)	1,443 (59.4)	357 (61.4)	516 (55.4)	398 (61.7)	172 (63.4)
Education (yr)	11.5 \pm 4.9	11.9 \pm 4.8	12.0 \pm 4.7	11.3 \pm 4.8	9.3 \pm 5.2
APOE4 carriers	931 (38.3)	150 (25.8)	394 (42.3)	321 (49.8)	66 (24.4)
Ligands (FMM/FBB)	1,378/1,050 (56.8/43.2)	208/373 (35.8/64.2)	613/318 (65.8/34.2)	323/322 (50.1/49.9)	69/202 (25.5/74.5)
MMSE	24.1 \pm 5.2	28.0 \pm 2.0	25.6 \pm 3.2	19.1 \pm 5.1	22.0 \pm 5.3

Values are presented as number (%) or mean \pm standard deviation.

CU: cognitively unimpaired, MCI: mild cognitive impairment, DAT: dementia of the Alzheimer's type, F: female, FBB: ¹⁸F-florbetaben, FMM: ¹⁸F-flutemetamol, MMSE: Mini-Mental State Examination.

Statistical analyses

The cutoff values for amyloid positivity on the dcCL and rdcCL scales for each brain region in the MR and CT datasets were determined using a Gaussian Mixture Model (GMM), a probabilistic machine learning method that models the data distribution as a mixture of multiple-Gaussian distributions. A GMM with 2 components ($k=2$) was fitted using the 'normalmixEM' function from the 'mixtools' R package (R Studio version 2023.12.1+402). The cutoff was defined as the point where the 2 Gaussian distributions intersect.

RESULTS

Demographics of the participants

Table 1 summarizes the demographic and clinical characteristics of the study participants. A total of 2,428 individuals were included in the analysis, with a mean age of 71.2 \pm 9.5 years. Among them, 1,443 (59.4%) were female, and the average years of education was 11.5 \pm 4.9. APOE4 carriers comprised 931 participants (38.3%). The PET ligands used in this study included 1,050 participants (43.2%) with FBB and 1,378 participants (56.8%) with FMM. The mean Mini-Mental State Examination (MMSE) score across all participants was 24.1 \pm 5.2. The APOE genotype information was unavailable for 53 patients, while education years were not recorded for 25 patients, and MMSE scores were not evaluated for 110 patients.

MRI-based CL cutoffs by brain regions

Table 2 summarizes the CL cutoffs identified for each region. The GMM analysis revealed distinct cutoffs for key regions associated with amyloid deposition. The calculated cutoffs were 28.5 for the global brain, 34.1 for the frontal cortex, 29.5 for the parietal cortex, 28.1 for the temporal cortex, 43.3 for the occipital cortex, 28.4 for the PC cortex, and 25.7 for the striatum (**Fig. 1**).

Table 2. Centiloid cutoffs identified for each brain region

Brain regions	Centiloid cutoff	
	MRI	CT
Global	28.5	29.5
Frontal cortex	34.1	32.4
Parietal cortex	29.5	36.6
Temporal cortex	28.1	20.8
Occipital cortex	43.3	28.7
Posterior cingulate cortex	28.4	39.0
Striatum	25.7	38.7

MRI: magnetic resonance imaging, CT: computed tomography.

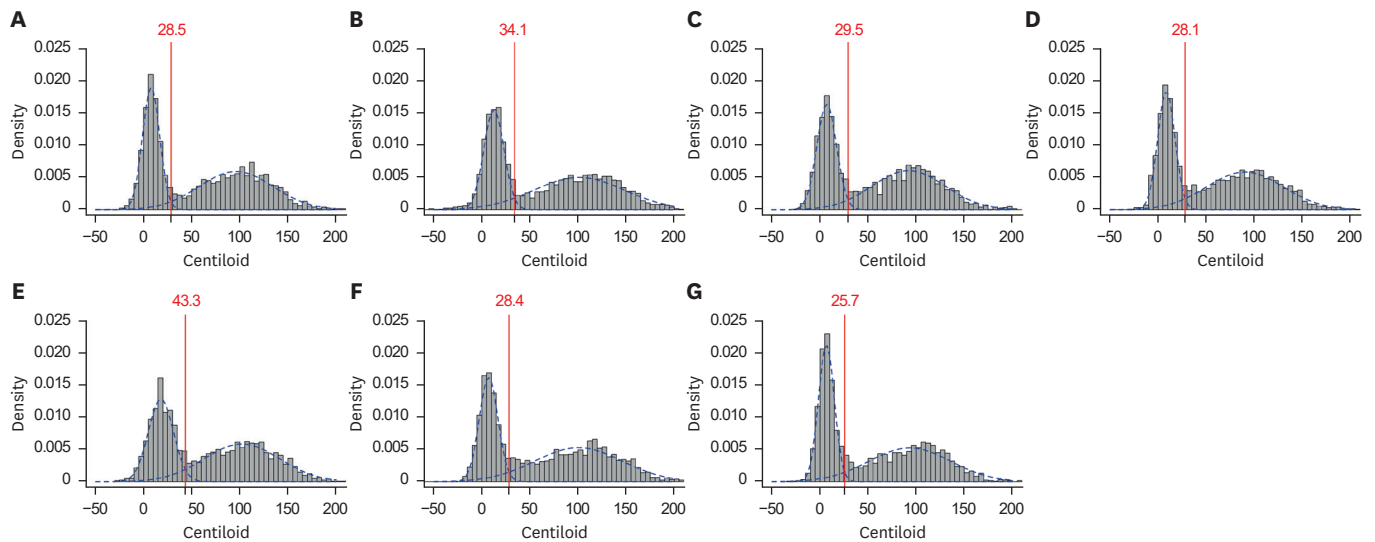


Fig. 1. Centiloid cutoff values derived from Gaussian Mixture Model using magnetic resonance method for each brain region: (A) Global, (B) Frontal, (C) Parietal, (D) Temporal, (E) Occipital, (F) Posterior cingulate, and (G) Striatum.

CT-based CL cutoffs by brain regions

Table 2 summarizes the cutoffs identified for each brain region. The GMM analysis revealed region-specific CL cutoffs, with cutoffs of 29.5 for the global brain, 32.4 for the frontal cortex, 36.6 for the parietal cortex, 20.8 for the temporal cortex, 28.7 for the occipital cortex, 39.0 for the PC cortex, and 38.7 for the striatum (**Fig. 2**).

Defining subgroups by global, regional, and striatal A β cutoffs

The cohort was classified into subgroups based on global, regional, and striatal A β cutoffs derived from MRI- and CT-based analyses. No significant differences were observed in A β positivity distributions between the MRI and CT-based methods across the subgroups (CU: $\chi^2=1.57$, p -value=0.67, MCI: $\chi^2=0.40$, p -value=0.40, DAT: $\chi^2=0.24$, p -value=0.97, and others:

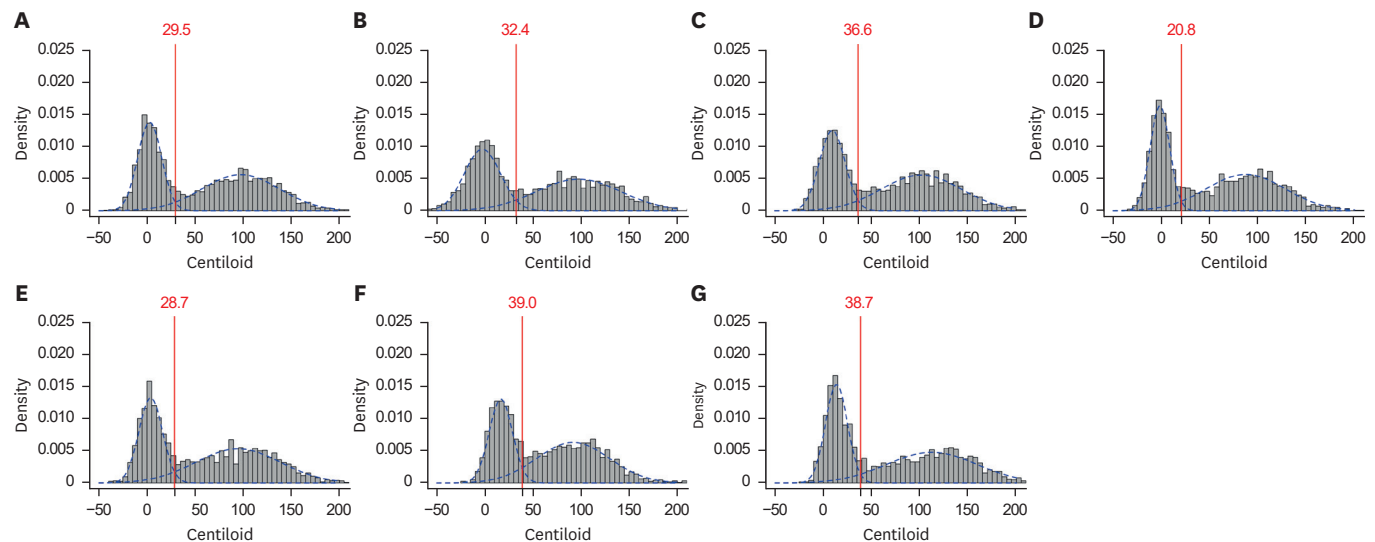


Fig. 2. Centiloid cutoff values derived from Gaussian Mixture Model using computed tomography method for each brain region: (A) Global, (B) Frontal, (C) Parietal, (D) Temporal, (E) Occipital, (F) Posterior cingulate, and (G) Striatum.

$\chi^2=2.65$, p -value=0.45). The proportions of each subgroup were further analyzed across the clinical diagnoses of CU, MCI, and DAT. Using MRI-based cutoffs (**Fig. 3A**), most CU participants were classified as G(-)R(-) (66.8%), followed by G(+)Str(+) (20.5%), G(-)R(+) (7.4%), and G(+)Str(-) (5.3%). Similarly, in the MCI group, the largest proportion was classified as G(+)Str(+) (53.9%), followed by G(-)R(-) (36.2%), G(-)R(+) (7.1%), and G(+)Str(-) (2.8%). Among DAT participants, the majority were G(+)Str(+) (85.9%), with smaller proportions in G(-)R(-) (9.1%), G(+)Str(-) (2.2%), and G(-)R(+) (2.8%). In comparison, using CT-based cutoffs (**Fig. 3B**), the distribution was slightly shifted. This difference in distribution appears to be due to variations in spatial resolution and tissue contrast between MRI and CT. Among CU participants, G(-)R(-) remained the largest group (67.6%), followed by G(+)Str(+) (18.6%), G(-)R(+) (9.0%), and G(+)Str(-) (4.8%). MCI participants showed a similar trend, with most classified as G(+)Str(+) (53.2%), followed by G(-)R(-) (36.2%), G(-)R(+) (7.8%), and G(+)Str(-) (2.8%). In the DAT group, G(+)Str(+) again dominated (85.6%), with smaller proportions classified as G(-)R(-) (9.0%), G(-)R(+) (3.3%), and G(+)Str(-) (2.2%) (**Table 3**). The PC cortex had the highest frequency of positivity in both CT-based (56.7%) and MRI-based (58.1%) cutoffs.

Table 3. Distribution of subgroups by clinical diagnosis and imaging modality

Variables	CU	MCI	DAT	Others
MRI				
G(-)R(-)	388 (66.8)	337 (36.2)	59 (9.1)	138 (50.9)
G(-)R(+)	43 (7.4)	66 (7.1)	18 (2.8)	22 (8.1)
G(+)Str(-)	31 (5.3)	26 (2.8)	14 (2.2)	10 (3.7)
G(+)Str(+)	119 (20.5)	502 (53.9)	554 (85.9)	101 (37.3)
CT				
G(-)R(-)	393 (67.6)	337 (36.2)	58 (9.0)	126 (46.5)
G(-)R(+)	52 (9.0)	73 (7.8)	21 (3.3)	28 (10.3)
G(+)Str(-)	28 (4.8)	26 (2.8)	14 (2.2)	16 (5.9)
G(+)Str(+)	108 (18.6)	495 (53.2)	552 (85.6)	101 (37.3)

Values are presented as number (%).

MRI: magnetic resonance imaging, CU: cognitively unimpaired, MCI: mild cognitive impairment, DAT: dementia of the Alzheimer's type, G: Global, Str: Striatal, R: Regional, CT: computed tomography.

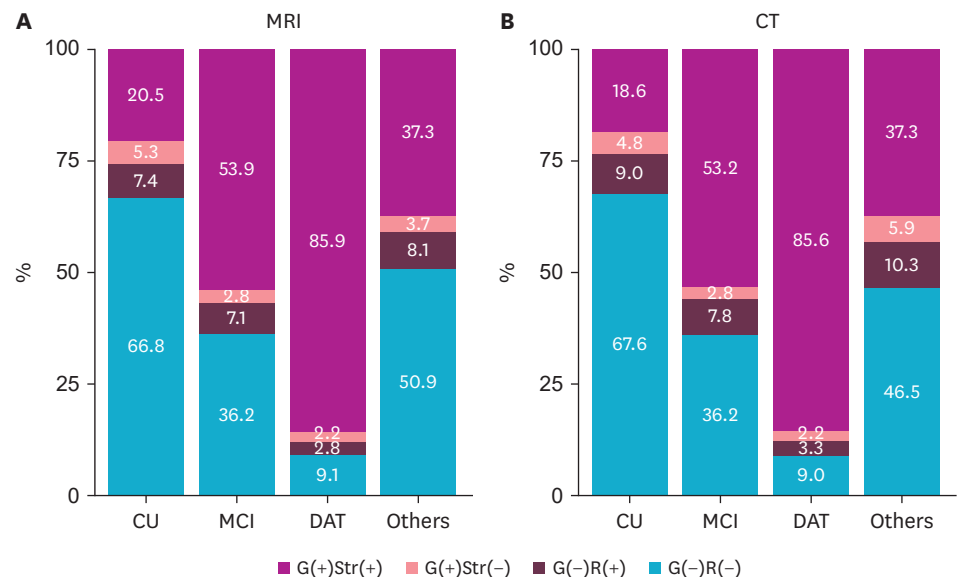


Fig. 3. Distribution of subgroups across clinical diagnoses based on (A) MRI- and (B) CT-derived amyloid-beta cutoffs. MRI: magnetic resonance imaging, CT: computed tomography, G: Global, Str: Striatal, R: Regional, CU: cognitively unimpaired, MCI: mild cognitive impairment, DAT: dementia of the Alzheimer's type.

DISCUSSION

In this study, we developed an algorithm to measure 3D T1 MRI-based and CT-based global and regional CLs using a large-sized dataset, enabling their broader applicability in clinical and research settings. This algorithm was used to calculate MRI-based and CT-based global and regional A β cutoffs through GMM, a statistical method. These cutoffs were then applied to classify participants into subgroups across cognitive stages (CU, MCI, and DAT) by global, regional, and striatal A β positivity, with similar proportions observed between MRI-based and CT-based methods. Taken together, our findings suggest that MRI-based and CT-based algorithms provide comparable classifications of A β uptakes across cognitive stages. These results highlight the potential to optimize resource allocation by reducing the need for additional 3D T1 MRI scans, making these algorithms highly practical for clinical and research applications.

Our study demonstrates that MRI-based and CT-based global A β cutoffs were generally similar, with the values closely aligning with previously reported MRI-based global A β cutoffs from other studies.³⁵⁻³⁷ While existing studies vary in their specific cutoff values, a liberal cutoff is often set around 20 and a conservative cutoff around 40, with most studies reporting values within this range.³⁸⁻⁴² Lower thresholds, typically around 10–20 CLs, are often used to detect early amyloid positivity,^{38,41,42} while higher thresholds, closer to 40 CLs, are associated with advanced amyloid burden seen in clinical stages of AD.^{39,40} These ranges are consistent with findings using common tracers such as FBB and FMM, highlighting the variability in cutoffs depending on the population characteristics and imaging methods employed.⁴³ This consistency highlights the reliability of our findings and supports the broader applicability of these cutoffs in clinical and research contexts.

For regional CLs, our ability to calculate accurate cutoffs was made possible by leveraging a head-to-head dataset incorporating young controls, which was established in our previous studies.^{19,44} These efforts led to the development of a commercialized product, BeauBrain Amylo, which enabled us to accurately derive regional CL values. This advantage allowed us to comprehensively compare MRI- and CT-based methods and establish robust regional cutoffs, revealing both similarities and differences between the two modalities. In some regions, such as the frontal cortex, the cutoffs were closely aligned between MRI and CT, whereas in others, like the occipital cortex and PC, notable differences were observed. These variations may reflect differences in the segmentation processes between MRI and CT algorithms, emphasizing the importance of modality-specific considerations in regional amyloid quantification.

These cutoffs were then applied to classify participants into subgroups across cognitive stages (CU, MCI, and DAT) by global, regional, and striatal A β positivity, with similar proportions observed between MRI-based and CT-based methods. The combined amyloid positivity rate [G(+)Str(+) and G(+)Str(-)] in our study was 25.8% and 23.4% for CU, 56.4% and 56.0% for MCI, and 88.1% and 87.8% for DAT in MRI-based and CT-based classifications, respectively. These rates closely align with previously reported amyloid positivity rates of approximately 20%–40% in CU individuals, 50%–60% in MCI, and over 80% in DAT, further validating the accuracy and reliability of our derived cutoffs. Interestingly, the G(-)R(+) subgroup was more frequently observed in non-dementia groups such as CU and MCI, while the G(+)Str(-) subgroup was more prevalent in CU compared to other cognitive stages. These patterns suggest potential transitional stages of amyloid

pathology, with G(-)R(+) possibly representing early amyloid accumulation detectable in regional brain areas, and G(+)Str(-) indicating global amyloid positivity without striatal involvement, often linked to advanced amyloid deposition.^{45,46}

Although these subgroups [G(-)R(+) and G(+)Str(-)] constitute a relatively small proportion of the cohort, their clinical significance warrants attention. Previous studies, including our own, have shown that individuals in the G(-)R(+) subgroup are more likely to progress to amyloid positivity over time, indicating its relevance as an early marker of amyloid pathology.^{16,18,47,48} Furthermore, both G(-)R(+) and G(+)Str(-) groups have been associated with intermediate levels of structural brain changes and cognitive impairments compared to fully amyloid-negative [G(-)R(-)] or fully amyloid-positive [G(+)Str(+)] groups.⁴⁹ For example, G(-)R(+) individuals may exhibit subtle cortical thinning, while G(+)Str(-) individuals demonstrate MCIs, consistent with early clinical stages of AD. These findings underscore the need for longitudinal studies to better understand the trajectory and implications of these subgroups, particularly in the context of early intervention and disease prevention.

Our study's primary strength lies in its use of a large, head-to-head dataset incorporating MRI- and CT-based imaging, enabling robust comparisons and accurate determination of both global and regional A β cutoffs. Despite this strength, our study has several limitations. First, the sample size for certain subgroups, such as G(-)R(+) and G(+)Str(-), was relatively small, which may limit the generalizability of findings for these categories. Second, the CT-based segmentation algorithm may have inherent biases compared to MRI-based methods, potentially affecting regional cutoff calculations. Third, while longitudinal data were used to validate some findings, further longitudinal analyses are needed to confirm the clinical trajectories of the defined subgroups. Fourth, the use of a specific PET tracer (e.g., FBB or FMM) may limit the generalizability of our findings to other tracers or cohorts with differing imaging protocols. Nevertheless, our study provides valuable insights into the comparability of MRI- and CT-based A β quantification, highlights the clinical significance of transitional subgroups such as G(-)R(+) and G(+)Str(-), and establishes a framework for integrating multimodal imaging in amyloid research, making it a valuable contribution to the field.

In summary, our study established robust MRI- and CT-based global and regional A β cutoffs, demonstrating their comparability and clinical utility across cognitive stages. These findings highlight the importance of transitional subgroups such as G(-)R(+) and G(+)Str(-) in understanding amyloid pathology and its progression. By providing a framework for multimodal amyloid quantification, our work contributes to advancing precision diagnostics and personalized therapeutic strategies in AD research.

REFERENCES

1. Sperling RA, Aisen PS, Beckett LA, Bennett DA, Craft S, Fagan AM, et al. Toward defining the preclinical stages of Alzheimer's disease: recommendations from the National Institute on Aging-Alzheimer's Association workgroups on diagnostic guidelines for Alzheimer's disease. *Alzheimers Dement* 2011;7:280-292. [PUBMED](#) | [CROSSREF](#)
2. Jack CR Jr, Andrews JS, Beach TG, Buracchio T, Dunn B, Graf A, et al. Revised criteria for diagnosis and staging of Alzheimer's disease: Alzheimer's Association workgroup. *Alzheimers Dement* 2024;20:5143-5169. [PUBMED](#) | [CROSSREF](#)
3. Jia J, Ning Y, Chen M, Wang S, Yang H, Li F, et al. Biomarker changes during 20 years preceding Alzheimer's disease. *N Engl J Med* 2024;390:712-722. [PUBMED](#) | [CROSSREF](#)

4. Li Y, Yen D, Hendrix RD, Gordon BA, Dlamini S, Barthélemy NR, et al. Timing of biomarker changes in sporadic Alzheimer's disease in estimated years from symptom onset. *Ann Neurol* 2024;95:951-965. [PUBMED](#) | [CROSSREF](#)
5. Clark CM, Pontecorvo MJ, Beach TG, Bedell BJ, Coleman RE, Doraiswamy PM, et al. Cerebral PET with florbetapir compared with neuropathology at autopsy for detection of neuritic amyloid- β plaques: a prospective cohort study. *Lancet Neurol* 2012;11:669-678. [PUBMED](#) | [CROSSREF](#)
6. Klunk WE, Engler H, Nordberg A, Wang Y, Blomqvist G, Holt DP, et al. Imaging brain amyloid in Alzheimer's disease with Pittsburgh compound-B. *Ann Neurol* 2004;55:306-319. [PUBMED](#) | [CROSSREF](#)
7. Klunk WE, Koeppe RA, Price JC, Benzinger TL, Devous MD Sr, Jagust WJ, et al. The Centiloid Project: standardizing quantitative amyloid plaque estimation by PET. *Alzheimers Dement* 2015;11:1-15.e1-4. [PUBMED](#) | [CROSSREF](#)
8. La Joie R, Ayakta N, Seeley WW, Borys E, Boxer AL, DeCarli C, et al. Multisite study of the relationships between antemortem [¹¹C]PIB-PET Centiloid values and postmortem measures of Alzheimer's disease neuropathology. *Alzheimers Dement* 2019;15:205-216. [PUBMED](#) | [CROSSREF](#)
9. Johnson KA, Sperling RA, Gidicsin CM, Carmasin JS, Maye JE, Coleman RE, et al. Florbetapir (F18-AV-45) PET to assess amyloid burden in Alzheimer's disease dementia, mild cognitive impairment, and normal aging. *Alzheimers Dement* 2013;9:S72-S83. [PUBMED](#) | [CROSSREF](#)
10. Jang H, Chun MY, Yun J, Kim JP, Kang SH, Weiner M, et al. Ethnic differences in the prevalence of amyloid positivity and cognitive trajectories. *Alzheimers Dement* 2024;20:7556-7566. [PUBMED](#) | [CROSSREF](#)
11. Jansen WJ, Janssen O, Tijms BM, Vos SJB, Ossenkoppele R, Visser PJ, et al. Prevalence estimates of amyloid abnormality across the Alzheimer disease clinical spectrum. *JAMA Neurol* 2022;79:228-243. [PUBMED](#) | [CROSSREF](#)
12. Rowe CC, Doré V, Jones G, Baxendale D, Mulligan RS, Bullich S, et al. ¹⁸F-florbetaben PET beta-amyloid binding expressed in Centiloids. *Eur J Nucl Med Mol Imaging* 2017;44:2053-2059. [PUBMED](#) | [CROSSREF](#)
13. Battle MR, Pillay LC, Lowe VJ, Knopman D, Kemp B, Rowe CC, et al. Centiloid scaling for quantification of brain amyloid with [¹⁸F]flutemetamol using multiple processing methods. *EJNMMI Res* 2018;8:107. [PUBMED](#) | [CROSSREF](#)
14. Navitsky M, Joshi AD, Kennedy I, Klunk WE, Rowe CC, Wong DF, et al. Standardization of amyloid quantitation with florbetapir standardized uptake value ratios to the Centiloid scale. *Alzheimers Dement* 2018;14:1565-1571. [PUBMED](#) | [CROSSREF](#)
15. Rowe CC, Jones G, Doré V, Pejoska S, Margison L, Mulligan RS, et al. Standardized expression of ¹⁸F-NAV4694 and ¹¹C-PiB β -amyloid PET results with the Centiloid scale. *J Nucl Med* 2016;57:1233-1237. [PUBMED](#) | [CROSSREF](#)
16. Kim SJ, Jang H, Yoo H, Na DL, Ham H, Kim HJ, et al. Clinical and pathological validation of CT-based regional harmonization methods of amyloid PET. *Clin Nucl Med* 2024;49:1-8. [PUBMED](#) | [CROSSREF](#)
17. Park CJ, Seo Y, Choe YS, Jang H, Lee H, Kim JP, et al. Predicting conversion of brain β -amyloid positivity in amyloid-negative individuals. *Alzheimers Res Ther* 2022;14:129. [PUBMED](#) | [CROSSREF](#)
18. Cho SH, Shin JH, Jang H, Park S, Kim HJ, Kim SE, et al. Amyloid involvement in subcortical regions predicts cognitive decline. *Eur J Nucl Med Mol Imaging* 2018;45:2368-2376. [PUBMED](#) | [CROSSREF](#)
19. Kim SJ, Ham H, Park YH, Choe YS, Kim YJ, Jang H, et al. Development and clinical validation of CT-based regional modified Centiloid method for amyloid PET. *Alzheimers Res Ther* 2022;14:157. [PUBMED](#) | [CROSSREF](#)
20. Rafii MS, Sperling RA, Donohue MC, Zhou J, Roberts C, Irizarry MC, et al. The AHEAD 3-45 study: design of a prevention trial for Alzheimer's disease. *Alzheimers Dement* 2023;19:1227-1233. [PUBMED](#) | [CROSSREF](#)
21. van Dyck CH, Swanson CJ, Aisen P, Bateman RJ, Chen C, Gee M, et al. Lecanemab in early Alzheimer's disease. *N Engl J Med* 2023;388:9-21. [PUBMED](#) | [CROSSREF](#)
22. Weiner MW, Veitch DP, Aisen PS, Beckett LA, Cairns NJ, Green RC, et al. The Alzheimer's Disease Neuroimaging Initiative 3: continued innovation for clinical trial improvement. *Alzheimers Dement* 2017;13:561-571. [PUBMED](#) | [CROSSREF](#)
23. Knopman DS, Lundt ES, Therneau TM, Albertson SM, Gunter JL, Senjem ML, et al. Association of initial β -amyloid levels with subsequent flortaucipir positron emission tomography changes in persons without cognitive impairment. *JAMA Neurol* 2021;78:217-228. [PUBMED](#) | [CROSSREF](#)
24. Cho SH, Choe YS, Kim HJ, Jang H, Kim Y, Kim SE, et al. A new Centiloid method for ¹⁸F-florbetaben and ¹⁸F-flutemetamol PET without conversion to PiB. *Eur J Nucl Med Mol Imaging* 2020;47:1938-1948. [PUBMED](#) | [CROSSREF](#)
25. Jang H, Shin D, Kim Y, Kim KW, Lee J, Kim JP, et al. Korea-Registries to Overcome Dementia and Accelerate Dementia Research (K-ROAD): a cohort for dementia research and ethnic-specific insights. *Dement Neurocogn Disord* 2024;23:212-223. [PUBMED](#) | [CROSSREF](#)

26. Christensen KJ, Moya J, Armson RR, Kern TM. Health screening and random recruitment for cognitive aging research. *Psychol Aging* 1992;7:204-208. [PUBMED](#) | [CROSSREF](#)
27. Ahn HJ, Chin J, Park A, Lee BH, Suh MK, Seo SW, et al. Seoul Neuropsychological Screening Battery-dementia version (SNSB-D): a useful tool for assessing and monitoring cognitive impairments in dementia patients. *J Korean Med Sci* 2010;25:1071-1076. [PUBMED](#) | [CROSSREF](#)
28. Albert MS, DeKosky ST, Dickson D, Dubois B, Feldman HH, Fox NC, et al. The diagnosis of mild cognitive impairment due to Alzheimer's disease: recommendations from the National Institute on Aging-Alzheimer's Association workgroups on diagnostic guidelines for Alzheimer's disease. *Alzheimers Dement* 2011;7:270-279. [PUBMED](#) | [CROSSREF](#)
29. McKhann GM, Knopman DS, Chertkow H, Hyman BT, Jack CR Jr, Kawas CH, et al. The diagnosis of dementia due to Alzheimer's disease: recommendations from the National Institute on Aging-Alzheimer's Association workgroups on diagnostic guidelines for Alzheimer's disease. *Alzheimers Dement* 2011;7:263-269. [PUBMED](#) | [CROSSREF](#)
30. van Straaten EC, Scheltens P, Knol DL, van Buchem MA, van Dijk EJ, Hofman PA, et al. Operational definitions for the NINDS-AIREN criteria for vascular dementia: an interobserver study. *Stroke* 2003;34:1907-1912. [PUBMED](#) | [CROSSREF](#)
31. Rascovsky K, Hodges JR, Knopman D, Mendez MF, Kramer JH, Neuhaus J, et al. Sensitivity of revised diagnostic criteria for the behavioural variant of frontotemporal dementia. *Brain* 2011;134:2456-2477. [PUBMED](#) | [CROSSREF](#)
32. McKeith IG, Boeve BF, Dickson DW, Halliday G, Taylor JP, Weintraub D, et al. Diagnosis and management of dementia with Lewy bodies: fourth consensus report of the DLB consortium. *Neurology* 2017;89:88-100. [PUBMED](#) | [CROSSREF](#)
33. Jang H, Jang YK, Kim HJ, Werring DJ, Lee JS, Choe YS, et al. Clinical significance of amyloid β positivity in patients with probable cerebral amyloid angiopathy markers. *Eur J Nucl Med Mol Imaging* 2019;46:1287-1298. [PUBMED](#) | [CROSSREF](#)
34. Kim SE, Woo S, Kim SW, Chin J, Kim HJ, Lee BI, et al. A nomogram for predicting amyloid PET positivity in amnesic mild cognitive impairment. *J Alzheimers Dis* 2018;66:681-691. [PUBMED](#) | [CROSSREF](#)
35. Doré V, Bullich S, Rowe CC, Bourgeat P, Konate S, Sabri O, et al. Comparison of ¹⁸F-florbetaben quantification results using the standard Centiloid, MR-based, and MR-less CapAIBL[®] approaches: validation against histopathology. *Alzheimers Dement* 2019;15:807-816. [PUBMED](#) | [CROSSREF](#)
36. Coath W, Modat M, Cardoso MJ, Markiewicz PJ, Lane CA, Parker TD, et al. Operationalizing the centiloid scale for [¹⁸F]florbetapir PET studies on PET/MRI. *Alzheimers Dement (Amst)* 2023;15:e12434. [PUBMED](#) | [CROSSREF](#)
37. Matsuda H, Ito K, Ishii K, Shimosegawa E, Okazawa H, Mishina M, et al. Quantitative evaluation of ¹⁸F-flutemetamol PET in patients with cognitive impairment and suspected Alzheimer's disease: a multicenter study. *Front Neurol* 2021;11:578753. [PUBMED](#) | [CROSSREF](#)
38. Amadoru S, Doré V, McLean CA, Hinton F, Shepherd CE, Halliday GM, et al. Comparison of amyloid PET measured in Centiloid units with neuropathological findings in Alzheimer's disease. *Alzheimers Res Ther* 2020;12:22. [PUBMED](#) | [CROSSREF](#)
39. Amariglio RE, Grill JD, Rentz DM, Marshall GA, Donohue MC, Liu A, et al. Longitudinal trajectories of the cognitive function index in the A4 study. *J Prev Alzheimers Dis* 2024;11:838-845. [PUBMED](#) | [CROSSREF](#)
40. Bullich S, Roé-Vellvé N, Marquié M, Landau SM, Barthel H, Villemagne VL, et al. Early detection of amyloid load using ¹⁸F-florbetaben PET. *Alzheimers Res Ther* 2021;13:67. [PUBMED](#) | [CROSSREF](#)
41. Farrell ME, Jiang S, Schultz AP, Properzi MJ, Price JC, Becker JA, et al. Defining the lowest threshold for amyloid-PET to predict future cognitive decline and amyloid accumulation. *Neurology* 2021;96:e619-e631. [PUBMED](#) | [CROSSREF](#)
42. Jack CR Jr, Wiste HJ, Weigand SD, Therneau TM, Lowe VJ, Knopman DS, et al. Defining imaging biomarker cut points for brain aging and Alzheimer's disease. *Alzheimers Dement* 2017;13:205-216. [PUBMED](#) | [CROSSREF](#)
43. Royse SK, Minhas DS, Lopresti BJ, Murphy A, Ward T, Koeppe RA, et al. Validation of amyloid PET positivity thresholds in Centiloids: a multisite PET study approach. *Alzheimers Res Ther* 2021;13:99. [PUBMED](#) | [CROSSREF](#)
44. Cho SH, Choe YS, Park S, Kim YJ, Kim HJ, Jang H, et al. Appropriate reference region selection of ¹⁸F-florbetaben and ¹⁸F-flutemetamol beta-amyloid PET expressed in Centiloid. *Sci Rep* 2020;10:14950. [PUBMED](#) | [CROSSREF](#)
45. Teipel SJ, Temp AGM, Levin F, Dyrba M, Grothe MJ; Alzheimer's Disease Neuroimaging Initiative. Association of PET-based stages of amyloid deposition with neuropathological markers of A β pathology. *Ann Clin Transl Neurol* 2021;8:29-42. [PUBMED](#) | [CROSSREF](#)

46. Thal DR, Rüb U, Orantes M, Braak H. Phases of A β -deposition in the human brain and its relevance for the development of AD. *Neurology* 2002;58:1791-1800. [PUBMED](#) | [CROSSREF](#)
47. Levin F, Jelistratova I, Betthausen TJ, Okonkwo O, Johnson SC, Teipel SJ, et al. *In vivo* staging of regional amyloid progression in healthy middle-aged to older people at risk of Alzheimer's disease. *Alzheimers Res Ther* 2021;13:178. [PUBMED](#) | [CROSSREF](#)
48. Hanseeuw BJ, Betensky RA, Mormino EC, Schultz AP, Sepulcre J, Becker JA, et al. PET staging of amyloidosis using striatum. *Alzheimers Dement* 2018;14:1281-1292. [PUBMED](#) | [CROSSREF](#)
49. Kim SE, Lee B, Park S, Cho SH, Kim SJ, Kim Y, et al. Clinical significance of focal β -amyloid deposition measured by ¹⁸F-flutemetamol PET. *Alzheimers Res Ther* 2020;12:6. [PUBMED](#) | [CROSSREF](#)